analytical chemistry

Article

pubs.acs.org/ac

Development of "Laser Ablation Direct Analysis in Real Time Imaging" Mass Spectrometry: Application to Spatial Distribution Mapping of Metabolites Along the Biosynthetic Cascade Leading to Synthesis of Atropine and Scopolamine in Plant Tissue

Kristen L. Fowble,[†] Kanae Teramoto,[‡] Robert B. Cody,[§] David Edwards,[§] Donna Guarrera,[§] and Rabi A. Musah*[,†]

[†]State University of New York at Albany, Department of Chemistry, 1400 Washington Avenue, Albany, New York 12222, United States

[‡]JEOL Ltd., 3-1-2 Musashino, Akishima, Tokyo, Japan 196-8558

[§]JEOL USA Inc., 11 Dearborn Road, Peabody, Massachusetts 01960, United States

Supporting Information

ABSTRACT: Methods for the accomplishment of small-molecule imaging by mass spectrometry are challenged by the need for sample pretreatment steps, such as cryo-sectioning, dehydration, chemical fixation, or application of a matrix or solvent, that must be performed to obtain interpretable spatial distribution data. Furthermore, these steps along with requirements of the mass analyzer such as high vacuum, can severely limit the range of sample types that can be analyzed by this powerful method. Here, we report the development of a laser ablation-direct analysis in real time imaging mass spectrometry approach which couples a 213 nm Nd:YAG solid state UV laser to a direct analysis in a real time ion source and high-resolution time-of-flight mass spectrometer. This platform enables facile determination of the spatial distribution of small-molecules spanning a range of polarities in a diversity of sample types and requires no matrix, vacuum, solvent, or complicated sample pretreatment steps. It furnishes high-resolution data, can be performed under ambient conditions on samples in their native form, and results in little to no fragmentation of analytes. We demonstrate its application through determination of the spatial distribution of molecules involved in the biosynthetic cascade leading to formation of the clinically relevant alkaloids atropine and scopolamine in *Datura leichhardtii* seed tissue.

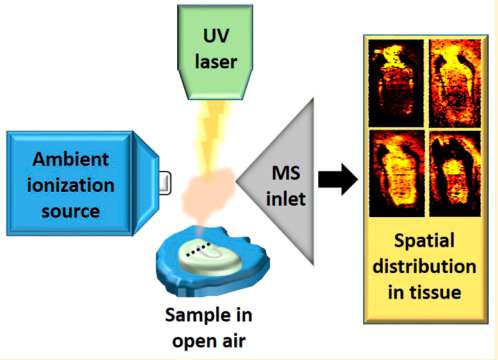

Recent significant advancements in imaging mass spectrometry (IMS) have provided a means whereby spatial distribution mapping of molecules within plant, animal and human tissues can be accomplished.[1] In this regard, much of the progress has been made in detecting macromolecules such as proteins, nucleic acids and other polymers, rather than small-molecules. The most well-established methods utilize a matrix-assisted laser desorption ionization (MALDI) source, although others such as secondary ion mass spectrometry (SIMS), liquid extraction surface analysis (LESA), laser ablation inductively coupled plasma (LA-ICP), desorption electrospray ionization (DESI), nano-DESI, laser ablation electrospray ionization (LAESI),[2] and their derivatives have also been successfully used for IMS. These approaches are complementary and, in general, each technique has specific sample pretreatment steps that if conducted improperly could dramatically impact the amount of useable data that can be acquired.[3] For this reason, successful experiments usually involve significant and often time-consuming methods development, and this in turn defines the sample types that can be analyzed. Until recently, the mapping of small-molecule distributions in biological matrixes was not easily achieved by these methods for a variety of reasons.[4] Imaging by MALDI was initially challenged by high background contributions from the matrix. In DESI analysis, the size of the charged droplet beam was too large relative to the area analyzed, and the data were poorly resolved. Some of these deficiencies have been overcome through advances in matrix deposition methods, mass analyzer enhancements, and charged droplet beam size reductions among other developments.[4] The continued need for high vacuum (SIMS, MALDI), the requirement of a matrix (MALDI), the need for a solvent (DESI, LAESI) which can be problematic in cases where the sample is sensitive to surface wetting, the optimization of multiple experimental parameters associated with ion source operation, ion suppression effects, limitations on the dielectric constant range of the compounds detected, and the require-

Received: October 21, 2016
Accepted: February 24, 2017
Published: February 24, 2017

DOI: 10.1021/acs.analchem.6b04137
Anal. Chem. 2017, 89, 3421−3429

ment for sophisticated sample preparation steps such as dehydration, chemical fixation and cryo-sectioning among others, present challenges to small-molecule imaging by these techniques. Even in cases such as matrix-free laser desorption ionization mass spectrometry (LDI-MS) or SIMS, the significant fragmentation of the analytes that occurs limits their application.[2,5] Although high mass measurements conducted by these techniques are extremely useful in biological studies, the need for a technique to routinely map the spatial distributions of small-molecules remains. Features of this technique could include the ability to (1) analyze the sample under ambient conditions with minimal to no sample pretreatment or need for solvent; (2) image irregular surfaces; (3) obtain high spatial resolution; (4) routinely detect a range of molecules of varying polarities; and (5) easily set up the experiment. In the case of plant tissue in particular, the ability of the technique to penetrate barriers, such as the cell wall, cuticle, or waxy surfaces, as well as to analyze both fresh and dried samples, would also be highly desirable.

We report here the development of a laser ablation direct analysis in real time imaging mass spectrometry (LADI-MS) platform that features several of the aforementioned advantages, and which can be used for the imaging of tissue distributions of small-molecules in both biological and nonbiological matrixes. The approach couples a UV laser with an ambient ionization direct analysis in real time (DART) ion source, interfaced with a time-of-flight (TOF) mass analyzer. Salient advantageous features of the method include little to no sample preparation steps, the ability to conduct the analysis under ambient conditions, good spatial resolution, the absence of the need for solvent, the ability to analyze irregularly shaped samples, and the ability to detect a broad range of molecules spanning the dielectric constant spectrum. The utility of the technique is demonstrated through illustration for the first time of the distribution within plant tissue, specifically *Datura leichhardtii* seed, of small-molecules related by their involvement in the sequential reactions leading to the production of the clinically relevant alkaloids atropine and scopolamine. The detected compounds, several of which have not been previously reported to be present in the species, are members of the tropane alkaloid class, and are biosynthesized by several members of the Solanaceae family, including *Atropa*, *Brugmansia*, *Datura*, *Duboisia*, *Hyoscyamus*, and *Mandragora*.[6−15]

EXPERIMENTAL SECTION

Seeds. Fifty *Datura leichhardtii* seeds were purchased from J. L Hudson, Seedsman (La Honda, CA).

Chemicals. High-purity helium was obtained from Airgas (Albany, NY). Phenylpyruvic acid, phenyllactic acid, and ornithine hydrochloride standards were purchased from Krackeler Scientific (Albany, NY). Scopolamine hydrobromide, atropine, tropinone, phenylalanine, arginine, and 2,5-dihydroxybenzoic acid (DHB) were purchased from Sigma-Aldrich (St. Louis, MO). Tropine was purchased from Alfa Aesar (Tewksbury, MA). Trifluoroacetic acid was purchased from Acros Organics (NJ).

Microscopy. A Nikon stereozoom SMZ800 microscope equipped with a Nikon DS Fi2 microscope camera was used to image the sagittal and transverse cross sections. Scanning electron microscopy was achieved using a JSM-IT300LV scanning electron microscope (JEOL USA, Peabody, MA). The seed cross sections were affixed to carbon glue on an SEM sampling block (JEOL USA, Peabody, MA) for imaging.

Sample Preparation for MALDI-MS/MS. An aqueous extract was prepared by slicing three *D. leichhardtii* seeds in half using a razor blade and submerging them in 50 μL of distilled water. The mixture was sonicated for 30 min. Solutions of authentic standards at a concentration of 10 mg/mL were made using 1% trifluoroacetic acid in water−acetonitrile (1:1).

MALDI-MS/MS Analysis. A matrix solution comprised of 10 mg/mL DHB in acetonitrile and 0.5% trifluoroacetic acid in water (1:1) was used. A mixture of 1 μL of aqueous seed extract in 10 μL of matrix solution was pipetted onto a stainless steel target plate. The sample was then allowed to dry in air. A JMS-S3000 SpiralTOF (JEOL, Tokyo, Japan) equipped with the TOF/TOF option was used for observation of MALDI mass spectra. Ions generated by irradiation with a 349 nm Nd:YLF laser were accelerated at 20 kV. Mass calibration of the seed extract was carried out by internal calibration using 5 peaks of PEG 200 ($[M + Na]^+$).

Sample Preparation for LADI-MS. A *D. leichhardtii* seed was cut in half, transverse wise, using a razor blade. The seed was deposited on a bed of LOCTITE silicone putty (Westlake, OH) to keep it stable, with the cut face exposed. The putty to which the seed had been affixed was then mounted on the sample plate within the laser system sample chamber.

LADI-MS Analysis. Ion images were acquired using an ESI NWR213 laser imaging system (ESI, Portland, OR) coupled with a direct analysis in real time (DART)-SVP ion source (IonSense, Saugus, MA) and JEOL AccuTOF mass spectrometer (JEOL USA, Peabody, MA). Spectra were collected at a rate of 2 scans/s. Spectra in the mass range of 60−800 m/z were acquired in positive ion mode at 350 °C. The ambient conditions set for the analyses included an orifice 1 voltage of 20 V and orifice 2 and ring lens voltages of 5 V each. The ion guide voltage was set to 600 V to allow for the analysis of ions over m/z 60. The mass spectrometer has a resolving power of 6000 fwhm. The rate of helium flow for the DART-SVP ion source was 2.0 L/min. Calibration was achieved using polyethylene glycol (PEG) as a reference standard. The dimensions of the area to be ablated were selected and the sample surface was ablated from left to right one line scan at a time at a constant velocity. At the end of each row there was a washout delay which served to prevent carry over of ions. It was arbitrarily set to 10 s, much longer than the actual washout time of 0.7 s. This was followed by an additional 10 s to allow the laser to reach the required fluence. TSSPro3 software (Shrader Software Solutions) was used for peak calibration and determining the peak centroid. Reconstructed ion chromatograms were created for each of the ions of interest and then exported to Excel files. The headings of the exported files were modified to correspond to the Agilent file format. Specifically, the scan numbers were removed and the time labels were converted from min to s. These updated Excel files were then imported into Iolite imaging software (University of Melbourne, Australia) (https://iolite-software.com/). This software enabled the coupling of the data file from the mass spectrometer to the text file created by the laser system to generate the ion images shown. Mass spectral analysis, elemental composition determination, and isotope analysis were performed using Mass Mountaineer software (Mass-spec-software.com, RBC Software, Portsmouth, NH).

Laser Ablation System and LADI-MS Seed Analysis. An ESI NWR213 computer-controlled solid state laser ablation system, which included a 213 nm Nd:YAG laser with a spot size range of 4−250 μm and a 100 mm × 10 mm, high performance

DOI: 10.1021/acs.analchem.6b04137
Anal. Chem. 2017, 89, 3421−3429

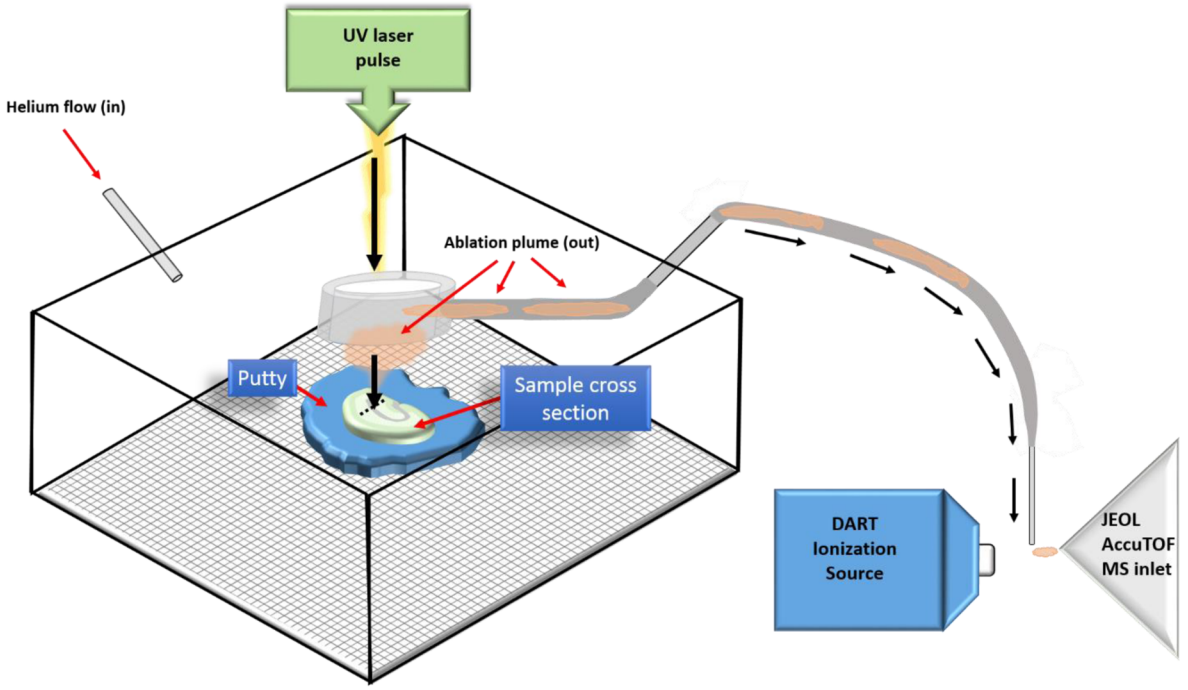

Figure 1. LADI mass spectrometry setup. A sample suspended in silicone putty is placed within the sample chamber of an ESI 213 Nd:YAG laser imaging platform. The chamber rests on an automated computer-controlled *x,y*-stage. Rastering the sample at constant speed beneath the laser pulse results in an ablation plume, which is transported via helium gas through tubing and directed to the open air space between the DART ion source and the inlet of the mass spectrometer.

TwoVol ablation chamber and high precision *x,y*-stage was used. The *D. leichhardtii* seed cross-section was placed in the system's airtight 800 mL sample chamber, which is mounted on a motorized, computer-controlled *x,y*-moveable stage. The stage platform can attain a depth of approximately 2 in., allowing for thick and irregularly shaped samples to be ablated. The window of the sample chamber is made of glass with an optical coating to minimize energy loss before the laser beam reaches the surface of the sample. The ESI NWR213 ablation system is equipped with a 1 mL ablation cup into which the ablation plume is directed from the sample chamber. Transport of the plume to the open air gap between the DART ion source and JEOL AccuTOF mass spectrometer inlet was accomplished using ultrahigh purity helium flowing at a constant rate into the sample chamber and out through Tygon tubing. Appended to the tubing was an open ended Corning Pyrex melting point capillary tube (VWR, Radnor, PA) positioned at the mass spectrometer inlet. The experimental setup is as depicted in Figure 1. Multiple laser parameters were optimized to achieve the strongest MS signals. These included laser beam energy density (fluence) = 21 J/cm^3; frequency = 20 Hz; scan speed = 50 μm/s; spot size = 50 × 50 μm^2; line width = 45 μm; and He flow rate = 600 mL/min. The fluence and spot size used represent the minimum values that permitted a sufficient enough amount of the seed to be ablated to detect a strong MS signal. The spot size was kept as small as possible to provide enough ablated seed material to the inlet, while maintaining good resolution. The scan rate was chosen to avoid oversampling of a given area on the one hand, while not rastering so quickly as to result in unablated areas. On the basis of the experimental parameters used, the spatial resolution attained was 110 × 50 μm^2 (i.e., [*x*-spot size + (cell washout time (0.7 s) × scan speed) + (DART-MS scan rate (1 s/2 scans) × scan speed)] × *y*-spot size).

RESULTS AND DISCUSSION

Microscopy of the Imaged Tissue. To assist with visualization of the spatial localization of observed masses, light and scanning electron microscopy (SEM) micrographs of both sagittal and transverse cross sections of *D. leichhardtii* seeds are presented in Figure 2. The mature seed is discoid in shape. The embryo, which is linear, adopts a loop (annular) configuration and is embedded within the endosperm. The seed coat (testa) is thickened in the region immediately surrounding the endosperm (an area known as the micropylar endosperm), and there is a cavity between the seed coat and micropylar endosperm. The curvature of the embryo results in the observation of two circles that are apparent in the transverse cross-section, representing the embryonic root (radical) and the stem between the radical and the cotyledon (i.e., the hypocotyl).[16] In these representations, the seed is oriented so that the micropylar testa appears at the top. For the LADI-MS analysis, a transverse cross-section of the seed was surveyed.

Tropane Alkaloid Biosynthesis. The comprehensiveness of the data set acquired in our experiments (described below), can be appreciated through consideration of what is known about the steps in atropine and scopolamine alkaloid biosynthesis in Solanaceae genera such as *Atropa*, *Brugmansia*, *Datura*, *Duboisia*, *Hyoscyamus* and *Mandragora*. It is believed to proceed by a common pathway that features the steps shown in Figure 3. Either ornithine or arginine can serve as the precursor from which putrescine is derived.[11,17,18] Transformation of arginine to putrescine involves the intermediacy of agmatine,[18] while formation of putrescine from ornithine is direct.[17] Putrescine is converted to *N*-methylputrescine via the action of putrescine *N*-methyltransferase.[12] The *N*-methylated amine is acted upon by *N*-methylputrescine oxidase which yields 4-methylaminobutanal, an aldehyde that undergoes spontaneous cyclization to form the *N*-methyl-Δ^1-pyrrolium cation.[19]

DOI: 10.1021/acs.analchem.6b04137
Anal. Chem. 2017, 89, 3421−3429

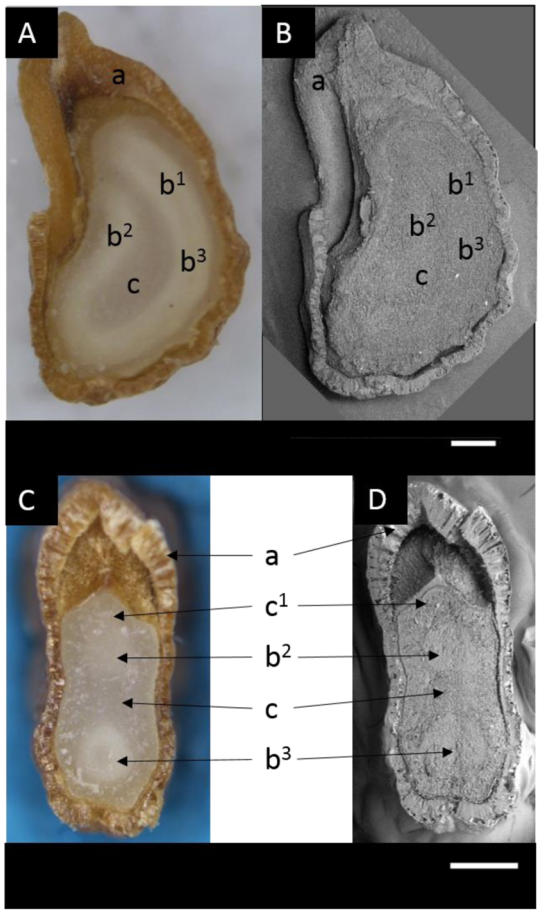

Figure 2. Light (A and C) and scanning electron microscopy (SEM) micrographs (B and D) of *Datura leichhardtii* seeds. Sagittal (top) and transverse (bottom) cross sections are presented. The scale bar shown in white corresponds to 500 μm in both cases.

Complexation of the cation with acetoacetic acid furnishes 4-(1-methyl-2-pyrrolidinyl)-3-oxobutanoate,[15] the immediate precursor of both hygrine[6] and tropinone.[15,14] Tropinone then undergoes either tropinone reductase I catalyzed conversion to tropine or transformation to pseudotropine,[20] which serves as the precursor to the polyhydroxylated calystegine[21] alkaloids A3, B1, or B2. Condensation of tropine with phenyllactic acid gives littorine.[22] Phenyllactic acid is biosynthesized from phenylalanine via phenylpyruvic acid.[23] Through the action of CYP80F1, littorine is converted into hyoscyamine aldehyde, which serves as the direct precursor of atropine (aka hyoscyamine).[13] Atropine then undergoes hyoscyamine 6-β-hydroxylase-mediated conversion to scopolamine via 6-β-hydroxyhyoscyamine.[24]

Ion Images Acquired by LADI-MS. Figure 4 shows color overlaid ion images acquired from analysis of a transverse section of a *D. leichhardtii* seed. These thumbnail renderings show the spatial distribution of the specified masses with their assigned molecular identities. They are arranged to emphasize the relationship to one another of the compounds they represent in the proposed biosynthetic cascade leading to the formation of atropine and scopolamine. The dashed line surrounding each image indicates the outer edge of the seed coat, and the 1 mm scale bar shown for arginine applies to all the ion images. The bar shown at the bottom of each ion image is a color spectrum (based on the empirical cumulative distribution function) ranging from black or dark red to yellow, indicating a low or zero intensity to a high relative intensity of the indicated ion. The ionization mechanism of DART-MS involves proton transfer to the analyte from protonated water clusters formed through the interaction of DART-derived metastable helium with atmospheric water. Thus, molecules with proton affinities greater than that of water can be ionized by this means. Furthermore, all things being equal, the greater the proton affinity of a given analyte, the greater will be the intensity of the detected ion. For this reason, relative ion intensities may not necessarily reflect the relative amounts of detected species. For example, one analyte may be of lower concentration than another, but if the former has a much higher proton affinity than the latter, its peak intensity will be greater. It is for this reason that the ion images shown in Figure 4 are not presented using the same color scale, as would usually be done in cases where the relative ion counts reflect the relative amounts of the detected ions. Thus, the color intensity scale for each ion image is independent of the others and only represents the relative intensity of the indicated ion throughout the seed half.

The mass spectrum depicted in the inset is representative of the micropylar endosperm, an area dominated by the presence of the ions represented in the gray panel in Figure 4. Other areas of the seed, such as the seed coat or embryo, produced spectra whose chemical fingerprint profiles were different from those of the micropylar endosperm (data not shown). The mass measurement data for the ions featured in this study are shown in Supporting Information Table S1. With the exception of the thumbnail which is enclosed in the black box (representing nominal m/z 381), the images that appear in the shaded area in Figure 4 represent high-intensity masses of unknown identity. That which appears in the box features an ion that is highly concentrated in the embryo, although it is of relatively low intensity. High-resolution masses corresponding to formulas consistent with the presence of protonated atropine, scopolamine, and the protonated forms of some of the intermediates so far reported to be involved in their biosynthesis in the Solanaceae (Figure 3) were observed. In some cases, the availability of authentic standards made it possible to confirm the tentative structural assignments by high-energy collision induced dissociation MS/MS experiments conducted using a JMS-S3000 JEOL SpiralTOF mass spectrometer (JEOL, Tokyo, Japan). These included the precursor arginine, the intermediates tropinone and tropine, and the end products atropine and scopolamine. These data are presented in Supporting Information Figures S1–S6. The ion images for the molecules confirmed to be present showed that they were compartmentalized within the seed tissue. High-resolution masses consistent with the presence of a number of other compounds known to be associated with tropane alkaloid biosynthesis such as *N*-methyl-Δ^1-pyrrolium cation, acetoacetic acid, 4-(1-methyl-2-pyrrolidinyl)-3-oxobutanoate, hygrine, pseudotropine, calystegines A3, B1, and B2, littorine, and hyoscyamine aldehyde were also observed. However, the absence of authentic standards precluded confirmation of their presence by MS/MS analysis. High-resolution masses consistent with ornithine, phenylalanine, phenylpyruvic acid, and phenyllactic acid were also observed. The identities of these masses could not be confirmed, however, because their

DOI: 10.1021/acs.analchem.6b04137
Anal. Chem. 2017, 89, 3421−3429

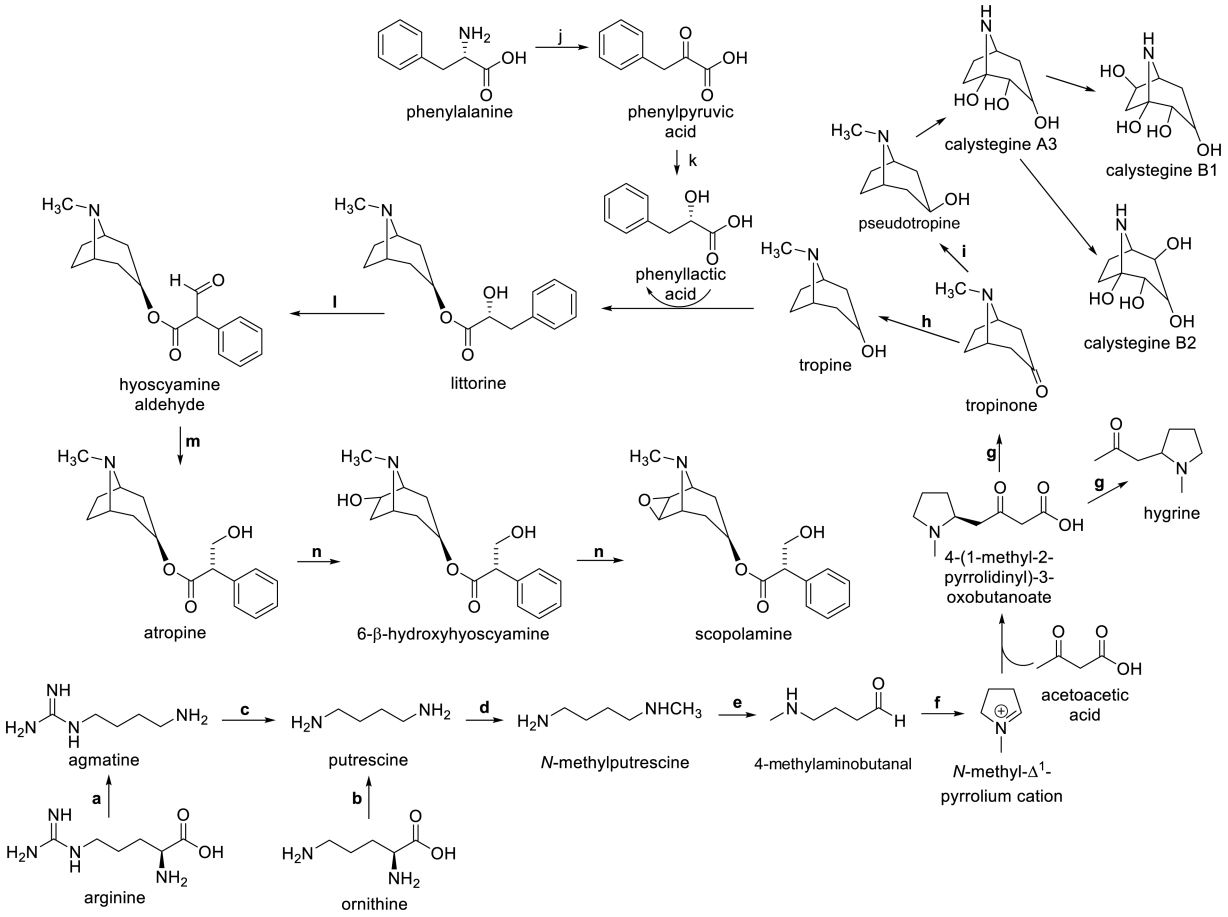

Figure 3. Proposed pathway for the biosynthesis of atropine and scopolamine in Solanaceae family plants. The enzymes known to be involved in the various steps are as follows: a = arginine decarboxylase, b = ornithine decarboxylase, c = agmatine ureohydrolase, d = putrescine *N*-methyltransferase; e = *N*-methylputrescine oxidase; f = spontaneous reaction, g = unknown enzyme, h = tropinone reductase I, i = tropinone reductase II, j = phenylalanine deaminase, k = lactate dehydrogenase, l = CYP80F1, m = alcohol dehydrogenase, and n = 6-β-hydroxylase.

intensities, even when using purified authentic standards with a variety of matrixes, were too weak to conduct MS/MS experiments. Thus, the ion images shown in the top panel are only of those compounds whose identities were confirmed by MS/MS analysis (Supporting Information Figures S1−S6).

Figure 5 utilizes artificially shaded SEM micrographs to provide a color-coded key that highlights the spatial distribution relationships between the observed masses. In these images, darker colors reflect higher levels of the detected masses. Several compounds were distributed throughout the tissue (indicated by red and pink shading in Figure 5A) including in the seed coat, all parts of the endosperm, and the visible embryo (i.e., radical and hypocotyl). Among the ions represented were the end product scopolamine (nominal m/z 304.1549) and its precursor atropine (m/z 290.1756). Littorine is a constitutional isomer of atropine. The absence of an analytical standard of littorine precluded definitive determination of its presence. The orange shading in Figure 5B shows the area of the amino acid arginine (m/z 175.1195). Its distribution was similar to that represented in Figure 5A, with the exception that it did not appear in the seed coat area that was proximal to the nonmicropylar endosperm. Tropine, the precursor to littorine, was more narrowly distributed, appearing as shown by blue shading in Figure 5C. It was concentrated in the micropylar testa, micropylar endosperm, and along the periphery of the endosperm to its midpoint. Tropinone (m/z 140.1075), the precursor of tropine, was distributed similarly (Figure 5, panel C).

There were several prominent masses of unknown identity that were also differentially distributed (see mass spectrum in Figure 4). These included one which appeared in the endosperm perimeter and the micropylar testa (m/z 163.0753, Figure 5D), some that were localized to the micropylar testa and the endosperm periphery, with small amounts in the radical (m/z 131.0492 and 179.0705, Figure 5E), one that was distributed throughout the endosperm and half of the seed coat (m/z 124.1116, Figure 5F), and one that was distributed throughout the tissue except in testa areas beyond the micropylar region (m/z 197.0812, Figure 5G). The compound represented by mass m/z 174.1113, which has the distribution shown in Figure 5B is also unknown. A mass of unknown identity at m/z 381.3340 was found to be located mostly in the embryo as well as surrounding endosperm and half of the seed coat (Figure 5H).

Within the past 5 years, a number of reports of MS-based imaging of seeds have appeared. These include spatial mapping of (1) lipids in *Camelina sativa* embryos,[25] rice grains[26] and cotton seeds;[27] (2) anthocyanins in black rice grains;[28] (3) a subset of amino acids and sugars in wheat;[29,30] and (4) hordatines in barley.[31] These studies were accomplished by MALDI- or DESI-MS imaging. The method described here is distinguished from these in that it does not require a matrix,

DOI: 10.1021/acs.analchem.6b04137
Anal. Chem. 2017, 89, 3421−3429

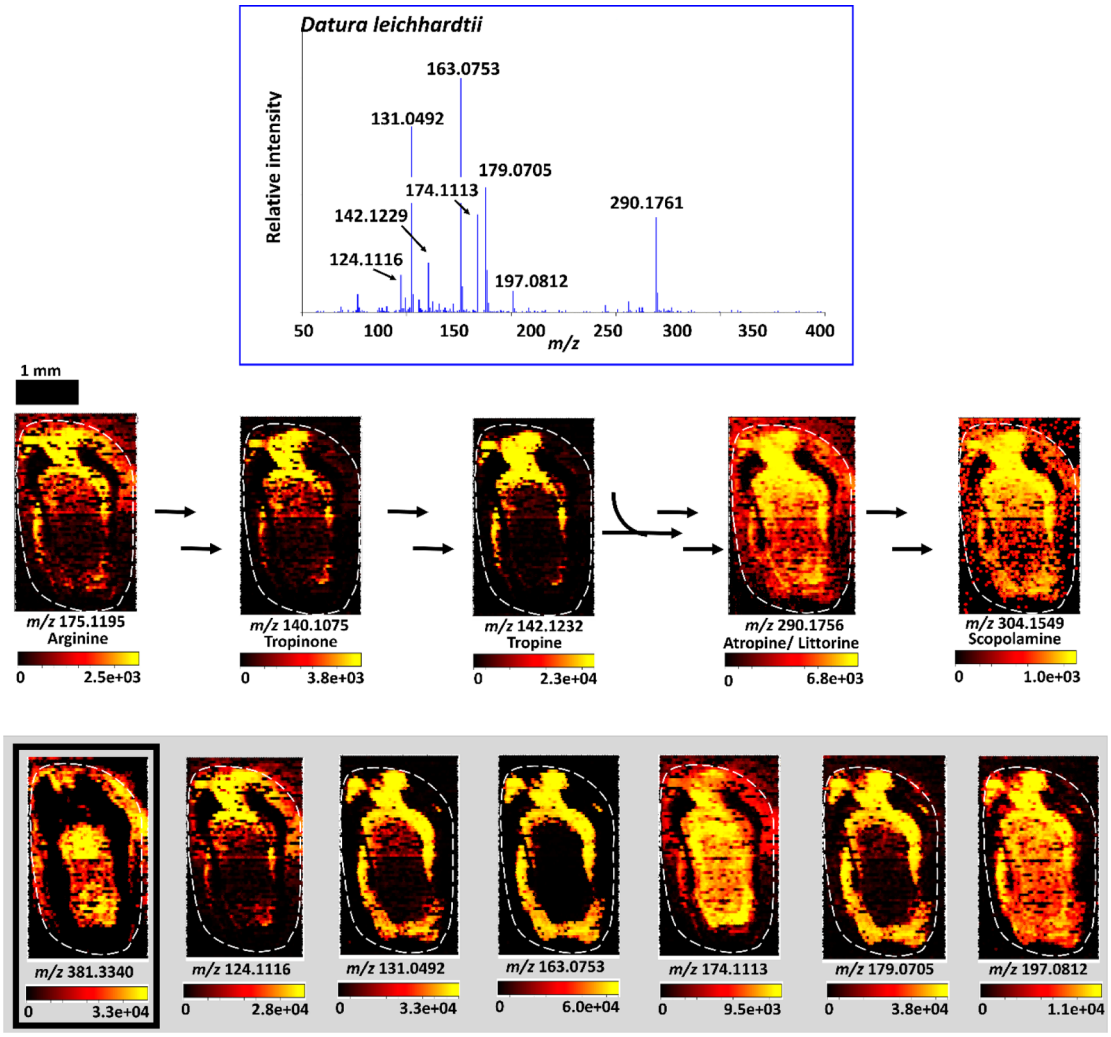

Figure 4. Color-overlaid ion images acquired from analysis of a transverse section of a *D. leichhardtii* seed by LADI-MS. The renderings show the spatial distribution of the specified masses. Assignments were confirmed by MS/MS analysis. The images are arranged to emphasize the relationship to one another of the compounds they represent in the biosynthetic cascade leading to the formation of atropine and scopolamine. The dashed line surrounding each image marks the outer edge of the seed coat, and the 1 mm scale bar shown for arginine applies to all the ion images. A typical DART mass spectrum representative of the area dominated by the unknown species (gray panel) is also presented. The mass measurement data for the ions featured are listed in Supporting Table S1. With the exception of the thumbnail which is enclosed in the black box, the images that appear in the gray-shaded area represent high-intensity masses of unknown identity. That which appears in the box features an ion (nominal m/z 381), which unlike the others featured, is highly concentrated in the embryo, although it is of relatively low intensity.

vacuum, or sample pretreatment steps such as cryosectioning, drying, or fixation in gelatin, carboxymethyl cellulose, or polyethylene glycol.[32] Recently, indirect DESI-IMS methods were used to detect atropine and scopolamine in *D. stramonium* leaf tissue,[33] malabaricone C in *Myristica malabarica* seed,[34] and rohitukline in *Dysoxylum binectariferum* seed.[35] This was done by creating an imprint of a leaf on a porous surface and scanning the imprint. Although these analyses were accomplished by an ambient ionization method, the approach contrasts with ours in that (1) the technique described here can be used to analyze dry sample surfaces directly with no need for solvent; and (2) the spot size achieved here was 50 μm and could be reduced to 10 μm. Furthermore, our method allowed direct analysis of the tissue and did not require solvent. This enabled detection of a much broader range of compounds, including several involved in a common metabolic cascade. IMS has also been accomplished under ambient conditions using an IR-laser coupled to a DART source, in contrast to the UV laser used in this work.[36] Another IMS ambient ionization method that features a low-temperature plasma probe has been reported.[37] Our technique contrasts with theirs in that the laser spot size used here defines the spatial resolution that can be achieved, while in their approach, the spatial resolution attainable is a function of the size of the probe.[37] Zhang et al.[38] have demonstrated that a platform comprised of a multi-wavelength laser and a DART source, coupled to a mass spectrometer can be used to detect dye and drug samples directly from TLC plates. However, its potential imaging capabilities were not reported.

MALDI-MS/MS was used to confirm the identities of several of the observed masses. However, this technique was not optimal for the imaging study described here because although several MALDI matrix compounds were evaluated, the ion current from specific target molecules measured by MALDI directly from the seed was too low to obtain high-quality MS/MS data. In addition, it was nearly impossible to consistently obtain thin homogeneous slices from the very hard seeds to permit high-quality imaging with the MALDI-TOF/TOF

DOI: 10.1021/acs.analchem.6b04137
Anal. Chem. 2017, 89, 3421−3429

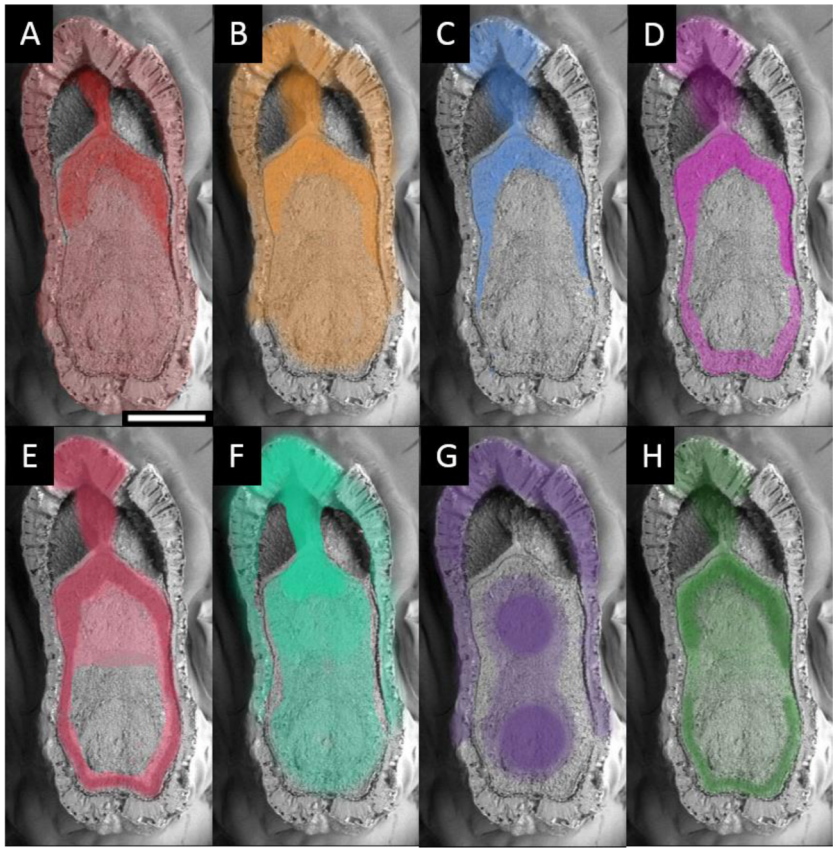

Figure 5. Illustration of differential distribution of detected ions as color overlays on the SEM micrograph of the transverse cross-section of the *D. leichhardtii* seed shown in Figure 2. The scale bar shown in white represents 500 μm and corresponds to all panels. The shading in each case shows the spatial distribution of various ions, with darker colors indicating greater ion intensity. (Panel A) m/z 290.1756 (atropine and/or littorine), m/z 304.1549 (scopolamine); (Panel B) m/z 174.1113 (unknown), m/z 175.1195 (arginine); (Panel C) m/z 140.1075 (tropinone), m/z 142.1232 (tropine); (Panel D) m/z 163.0753 (unknown); (Panel E) m/z 131.0492 (unknown), m/z 179.0705 (unknown); (Panel F) m/z 124.1116 (unknown); (Panel G) m/z 381.3340 (unknown); (Panel H) m/z 197.0812 (unknown).

system. While it may be possible to overcome these limitations with sufficient effort, we were able to circumvent these and other challenges often encountered with small-molecule imaging by conventional IMS approaches, by transporting the ablation plume created by the laser under atmospheric conditions, through tubing to a DART ion source in open air, and directing the ionized sample to the MS inlet. We chose to use MALDI-MS/MS to confirm the presence of the compounds of interest from seed extracts, which were much more conveniently analyzed by this method and which provided higher analyte concentrations and better spectral quality.

The assignments made for the compounds represented by the observed masses are based not only on the observations presented in this study but also on the very well-established chemistry associated with tropane alkaloid biosynthesis in plants, including *Datura* species.[6−15] However, the details regarding localization of tropane alkaloid-related compounds in plant tissue is poorly understood. The LADI-MS derived data not only show that compounds with exact masses consistent with those established in the literature to be observed in *Datura* seeds are present, but it also indicates their specific spatial distributions in the seed. In addition, the MALDI-MS/MS measurements furnished results that were consistent with the assignments for a number of specific compounds in the seeds whose involvement in tropane alkaloid biosynthesis is well-known.

Cell-specific accumulation of alkaloids in plants, a phenomenon proposed to protect tissues from the often cytotoxic effects of these compounds, is a well-known occurrence,[39,40,9,41] and compartmentalization of scopolamine, atropine, and other related alkaloids in both roots and aerial tissues has been observed.[42,43] However, visual demonstration of differential tissue distribution of this range of small-molecules related by their involvement in a common metabolic cascade in seeds or other plant tissues has not been reported. The intermediates, enzymes and end products in alkaloid synthesis are thought to be translocated within cells as well as between different cell types located in various tissues.[44] In *Atropa belladonna* and *Hysocyamus muticus* plants, the enzymes required for the biosynthesis of the alkaloids atropine and scopolamine are located differentially throughout the plant tissue.[41] The two enzymes located at the first and last steps of the biosynthetic cascade are found in the plant roots, while enzymes involved in intermediate steps are located within different cell types. Thus, their alkaloid substrates are accordingly differentially distributed, and some trafficking must occur between tissues and cell types in order for the biosynthetic cascade leading to alkaloid end products to progress. Previous reports have demonstrated that tropane alkaloid biosynthesis occurs in the roots[10] and that the compounds are subsequently translocated to other plant parts in low amounts. Since they appeared in high concentrations in the seeds, they are either transported there during seed development, synthesized within the seed during its

DOI: 10.1021/acs.analchem.6b04137
Anal. Chem. 2017, 89, 3421−3429

development, or perhaps both. Although it has been postulated that the alkaloids have a chemical defense function,[7,45] one intriguing possibility is that they are required for seed germination. In support of this hypothesis, it has been observed that during germination of *D. stramonium* seeds, the amounts of atropine and scopolamine decrease immediately after the seeds are moistened with water and drop to undetectable levels until 4 days after germination, at which point the levels increase dramatically.[46] Since neither compound was detected in the germination medium, it was suggested that these alkaloids were in some way utilized in metabolic processes related to the growth of the cotyledon. Further studies will be required to investigate this hypothesis.

CONCLUSIONS

The method described here permits access to small-molecule ion images of tissues in a fashion that circumvents some of the inherent challenges of other IMS methods. Because of the capabilities of the DART source, no vacuum, solvent, fixatives, matrix, or ion beam was required. Flat samples could be affixed to carbon tape for analysis, and oddly shaped samples such as the seeds that were surveyed here could be suspended in silicone putty to keep them level and immovable. The lower limit of the laser spot size for which the molecules of interest were readily detected by the mass analyzer used here was 10 μm (data not shown). The setup was comprised entirely of commercially available components, and it was easy to assemble.

The observed spatial distribution profiles of the analyzed seeds imply the presence of highly refined inter- and intracellular small-molecule transport machinery in order to accomplish and retain compartmentalization as well as traffic substrates to locations where they can react with other partners or serve as precursors to form other molecules. Furthermore, the results hint at the likely locales of the enzymes involved in the biosynthesis of the observed compounds. Of potential practical utility is the identification of tissues in which economically important natural products are concentrated. This information could be exploited for the development of efficient and streamlined isolations protocols that might prove to be more economically viable than current approaches. The method is broadly applicable and could be used to interrogate a range of sample types.

ASSOCIATED CONTENT

Supporting Information

The Supporting Information is available free of charge on the ACS Publications website at DOI: 10.1021/acs.analchem.6b04137.

Mass measurement data for a *D. leichhardtii* seed and MALDI-MS/MS confirmation of featured ions (PDF)

AUTHOR INFORMATION

Corresponding Author

*E-mail: rmusah@albany.edu.

ORCID

Rabi A. Musah: 0000-0002-3135-4130

Notes

The authors declare the following competing financial interest(s): K.T., R.B.C., D.E., and D.G. are employed by JEOL, the manufacturer of the scanning electron microscope and mass spectrometers used in this study.

ACKNOWLEDGMENTS

The financial support of the National Science Foundation (NSF) to R.A.M. and R.B.C. (Grant 1310350), Grant 1429329 from the NSF to R.A.M., and a grant to R.A.M. from the National Institute of Justice (Grant 2015-DN-BX-K057) are gratefully acknowledged. Thanks are extended to Electro Scientific Industries for use of the Nd:YAG laser. This project was supported by Award No. 2015-DN-BX-K057, awarded by the National Institute of Justice, Office of Justice Programs, U.S. Department of Justice. The opinions, findings, and conclusions or recommendations expressed in this publication/program/exhibition are those of the author(s) and do not necessarily reflect those of the Department of Justice.

REFERENCES

(1) Bodzon-Kulakowska, A.; Suder, P. *Mass Spectrom. Rev.* **2016**, *35*, 147−169.

(2) Kiss, A.; Hopfgartner, G. *Methods* **2016**, *104*, 142−153.

(3) Dong, Y.; Li, B.; Malitsky, S.; Rogachev, I.; Aharoni, A.; Kaftan, F.; Svatoš, A.; Franceschi, P. *Front. Plant Sci.* **2016**, DOI: 10.3389/fpls.2016.00060.

(4) Brown, V. L.; He, L. In *Mass Spectrometry Imaging of Small Molecules*; He, L., Ed.; Springer: New York, 2015; pp 1−7.

(5) Heeren, R. M. A.; McDonnell, L. A.; Amstalden, E.; Luxembourg, S. L.; Altelaar, A. F. M.; Piersma, S. R. *Appl. Surf. Sci.* **2006**, *252*, 6827−6835.

(6) Abraham, T. W.; Leete, E. *J. Am. Chem. Soc.* **1995**, *117*, 8100−8105.

(7) Alves, M. N.; Sartoratto, A.; Trigo, J. R. *J. Chem. Ecol.* **2007**, *33*, 297−309.

(8) Berkov, S.; Philipov, S. *Pharm. Biol.* **2002**, *40*, 617−621.

(9) Berkov, S.; Zayed, R.; Doncheva, T. *Fitoterapia* **2006**, *77*, 179−182.

(10) Hashimoto, T.; Hayashi, A.; Amano, Y.; Kohno, J.; Iwanari, H.; Usuda, S.; Yamada, Y. *J. Biol. Chem.* **1991**, *266*, 4648−4653.

(11) Hashimoto, T.; Yukimune, Y.; Yamada, Y. *Planta* **1989**, *178*, 131−137.

(12) Hibi, N.; Fujita, T.; Hatano, M.; Hashimoto, T.; Yamada, Y. *Plant Physiol.* **1992**, *100*, 826−835.

(13) Li, R.; Reed, D. W.; Liu, E.; Nowak, J.; Pelcher, L. E.; Page, J. E.; Covello, P. S. *Chem. Biol.* **2006**, *13*, 513−520.

(14) Portsteffen, A.; Draeger, B.; Nahrstedt, A. *Phytochemistry* **1992**, *31*, 1135−1138.

(15) Robins, R. J.; Abraham, T. W.; Parr, A. J.; Eagles, J.; Walton, N. J. *J. Am. Chem. Soc.* **1997**, *119*, 10929−10934.

(16) Gunn, C. R., Gaffney, F. B. *Seed Characteristics of 42 Economically Important Species of Solanaceae in the United States*, United States Department of Agriculture Technical Bulletin 1471; United States Department of Agriculture: Washington, DC, 1974.

(17) Leete, E. *J. Am. Chem. Soc.* **1962**, *84*, 55−57.

(18) Walton, N. J.; Robins, R. J.; Peerless, A. C. J. *Planta* **1990**, *182*, 136−141.

(19) Katoh, A.; Shoji, T.; Hashimoto, T. *Plant Cell Physiol.* **2007**, *48*, 550−554.

(20) Hashimoto, T.; Nakajima, K.; Ongena, G.; Yamada, Y. *Plant Physiol.* **1992**, *100*, 836−845.

(21) Scholl, Y.; Schneider, B.; Dräger, B. *Phytochemistry* **2003**, *62*, 325−332.

(22) Bedewitz, M. A.; Góngora-Castillo, E.; Uebler, J. B.; Gonzales-Vigil, E.; Wiegert-Rininger, K. E.; Childs, K. L.; Hamilton, J. P.; Vaillancourt, B.; Yeo, Y.-S.; Chappell, J.; DellaPenna, D.; Jones, A. D.; Buell, C. R.; Barry, C. S. *Plant Cell* **2014**, *26*, 3745−3762.

(23) Lakshmi Prasuna, M.; Mujahid, M.; Sasikala, C.; Ramana, C. V. *Microbiol. Res.* **2012**, *167*, 526−531.

DOI: 10.1021/acs.analchem.6b04137
Anal. Chem. 2017, 89, 3421−3429

(24) Hashimoto, T.; Matsuda, J.; Yamada, Y. *FEBS Lett.* **1993**, *329*, 35−39.
(25) Horn, P. J.; Silva, J. E.; Anderson, D.; Fuchs, J.; Borisjuk, L.; Nazarenus, T. J.; Shulaev, V.; Cahoon, E. B.; Chapman, K. D. *Plant J.* **2013**, *76*, 138−150.
(26) Zaima, N.; Goto-Inoue, N.; Hayasaka, T.; Setou, M. *Rapid Commun. Mass Spectrom.* **2010**, *24*, 2723−2729.
(27) Horn, P. J.; Korte, A. R.; Neogi, P. B.; Love, E.; Fuchs, J.; Strupat, K.; Borisjuk, L.; Shulaev, V.; Lee, Y.-J.; Chapman, K. D. *Plant Cell* **2012**, *24*, 622−636.
(28) Yoshimura, Y.; Zaima, N.; Moriyama, T.; Kawamura, Y. *PLoS One* **2012**, *7*, e31285.
(29) Burrell, M.; Earnshaw, C.; Clench, M. *J. Exp. Bot.* **2007**, *58*, 757−763.
(30) Walker, H. J.; Steels, C.; Bendell, L.; Clench, M. R.; Read, D. J.; Cameron, D. D.; Burrell, M. M. *Proteomics* **2016**, *16*, 1690−1694.
(31) Gorzolka, K.; Bednarz, H.; Niehaus, K. *Planta* **2014**, *239*, 1321−1335.
(32) Peukert, M.; Matros, A.; Lattanzio, G.; Kaspar, S.; Abadía, J.; Mock, H.-P. *New Phytol.* **2012**, *193*, 806−815.
(33) Thunig, J.; Hansen, S. H.; Janfelt, C. *Anal. Chem.* **2011**, *83*, 3256−3259.
(34) Ifa, D. R.; Srimany, A.; Eberlin, L. S.; Naik, H. R.; Bhat, V.; Cooks, R. G.; Pradeep, T. *Anal. Methods* **2011**, *3*, 1910−1912.
(35) Mohana Kumara, P.; Srimany, A.; Ravikanth, G.; Uma Shaanker, R.; Pradeep, T. *Phytochemistry* **2015**, *116*, 104−110.
(36) Galhena, A. S.; Harris, G. A.; Nyadong, L.; Murray, K. K.; Fernández, F. M. *Anal. Chem.* **2010**, *82*, 2178−2181.
(37) Liu, Y.; Ma, X.; Lin, Z.; He, M.; Han, G.; Yang, C.; Xing, Z.; Zhang, S.; Zhang, X. *Angew. Chem., Int. Ed.* **2010**, *49*, 4435−4437.
(38) Zhang, J.; Zhou, Z.; Yang, J.; Zhang, W.; Bai, Y.; Liu, H. *Anal. Chem.* **2012**, *84*, 1496−1503.
(39) St-Pierre, B.; Vazquez-Flota, F. A.; De Luca, V. *Plant Cell* **1999**, *11*, 887−900.
(40) Bird, D. A.; Franceschi, V. R.; Facchini, P. J. *Plant Cell* **2003**, *15*, 2626−2635.
(41) Ziegler, J.; Facchini, P. J. *Annu. Rev. Plant Biol.* **2008**, *59*, 735−769.
(42) Berkov, S.; Philipov, S. *Pharm. Biol.* **2002**, *40*, 617−621.
(43) Zayed, R.; Wink, M.; El-Shamy, H. *Z. Naturforsch., C: J. Biosci.* **2006**, *61*, 560.
(44) Roze, L. V.; Chanda, A.; Linz, J. E. *Fungal Genet. Biol.* **2011**, *48*, 35−48.
(45) Kariñho-Betancourt, E.; Agrawal, A. A.; Halitschke, R.; Núñez-Farfán, J. *New Phytol.* **2015**, *206*, 796−806.
(46) Yoneda, K.; Suzuki, S.; Kusu, H. *Shoyakugaku Zasshi* **1992**, *46*, 352−357.

DOI: 10.1021/acs.analchem.6b04137
Anal. Chem. 2017, 89, 3421−3429